Chemical Physics 573 (2023) 111977

Contents lists available at ScienceDirect

Chemical Physics

journal homepage: www.elsevier.com/locate/chemphys

Vibrational spectra of chiral 3FmX$_1$PhX$_2$6 homologues (m = 5, 6; X$_1$ = H, f; X$_2$ = F) in isotropic liquid, smectic and crystal phases

Aleksandra Deptuch [a,*], Natalia Górska [b], Monika Srebro-Hooper [b], James Hooper [b], Magdalena Dziurka [b], Magdalena Urbańska [c]

[a] Institute of Nuclear Physics Polish Academy of Sciences, Radzikowskiego 152, PL-31342 Kraków, Poland
[b] Faculty of Chemistry, Jagiellonian University, Gronostajowa 2, PL-30387 Kraków, Poland
[c] Institute of Chemistry, Military University of Technology, Kaliskiego 2, PL-00908 Warsaw, Poland

ARTICLE INFO

Keywords:
Fourier-transform infra-red spectroscopy
Smectic liquid crystals
Glass
Hydrogen bonds

ABSTRACT

The IR spectra of four liquid crystalline, partially fluorinated compounds are investigated as a function of temperature. The band assignments are based on dispersion-corrected density functional calculations, performed with the BLYP-def2SVP and BLYP-def2TZVP methods, on the isolated molecules in two different conformations. The scaling parameter between the experimental and calculated wavenumbers is obtained. The def2SVP basis set gives better agreement of the computed wavenumbers with the experimental wavenumbers. Although the def2TZVP basis set leads to an underestimation of the wavenumbers, it reproduces correctly the splitting of the absorption bands arising from the stretching of the C═O bonds. The temperature dependence of the νC═O bands indicates the formation of the hydrogen bonds between molecules on cooling, although no dramatic change is observed during vitrification of the smectic C$_A$* phase.

1. Introduction

Infra-red (IR) spectroscopy is a widely used tool in organic chemistry for investigating intra-molecular vibrations, and it is consequently applied, among other practices, to ascertain the structure of products and the purity of compounds, to determine the extent of inter-molecular interactions, to observe the dependence of particular vibrational modes on temperature and phase transitions, and to identify decomposition products [1–16]. The aim of this study is to compare the IR spectra of four chiral compounds from the 3FmX$_1$PhX$_2$6 family, which exhibit chiral smectic liquid phases that include the antiferroelectric smectic C$_A$* (SmC$_A$*), ferroelectric SmC*, and paraelectric SmA* phases [15–18], and the SmC$_\alpha$* sub-phase [19]. The molecules of selected compounds differ in the length of the non-chiral terminal chain (m = 5 or 6) and/or by fluorosubstitution of the benzene ring (X$_1$ = H or F; X$_2$ = F), but the length of the terminal C$_r$H$_{2r+1}$ chain (r = 6) is kept constant, as presented in Fig. 1. Accordingly, the simplified mX$_1$X$_2$6 abbreviation is used herein instead of the 3FmX$_1$PhX$_2$6 form. The phase transition temperatures for the investigated compounds are collected in Table 1. Although the IR spectra of these compounds at room temperature have already been reported [6], their temperature dependence and full computational assignment have not been investigated yet.

During cooling at 3–20 K/min, the 5HF6 and 6HF6 compounds form the vitrified SmC$_A$* phase, and the crystal phase appears subsequently upon heating (cold crystallization). The glass transition temperature T_g increases strongly with the increasing cooling rate, while it is rather constant for different heating rates and equal to 233 K for 5HF6 and 234 K for 6HF6 [18]. The 6FF6 compound, on the other hand, crystallizes at rather small undercooling [20], while the 5FF6 compound shows the intermediate properties, as its crystallization occurs slowly and can be avoided for cooling rates ≥ 10 K/min [19,21]. Similar influence of fluorosubstitution at the X$_1$, X$_2$ positions was observed previously for the 7HF6 and 7FF6 pair, the former being a glassformer and the latter crystallizing during cooling at the 20 K/min rate [15]. Furthermore, the FT-IR results showed a shift in the wavenumbers of two out of three absorption bands related to the C═O stretching in the 7FF6 molecule compared to 7HF6 [15]. As it is however not clear whether there is a connection between the vibrational dynamics and glassforming properties, it is thus necessary to investigate the temperature dependence of FT-IR spectra for similar compounds to establish the extent of intra-molecular interactions and conformational disorder in various thermodynamic states. The extensive study of the glass transition and

* Corresponding author.
E-mail address: aleksandra.deptuch@ifj.edu.pl (A. Deptuch).

https://doi.org/10.1016/j.chemphys.2023.111977
Received 29 March 2023; Received in revised form 30 May 2023; Accepted 31 May 2023
Available online 5 June 2023

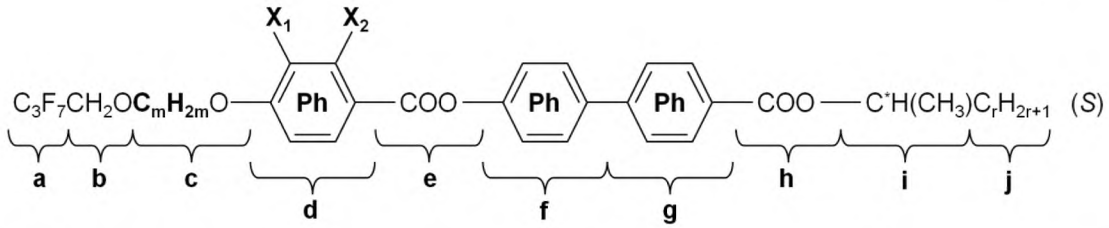

Fig. 1. General molecular formula of the 3FmX$_1$PhX$_2$r (or shorter mX$_1$X$_2$r) series. The a-j letters denote the particular moieties, which are used in the band assignments of the IR spectra. This study includes compounds with m = 5, 6; X$_1$ = H, F; X$_2$ = F, r = 6 and the mX$_1$X$_2$6 abbreviation will be further used.

Table 1
Phase transition temperatures, in K, for four mX$_1$X$_2$6 compounds, determined on heating [16,18,19]. Cr – crystal phase, Iso – isotropic liquid. The presence and absence of a phase are denoted by a bullet '•' and dash '–', respectively.

System	Ref.	Cr		SmC$_A$*		SmC*		SmC$_\alpha$*		SmA*		Iso
5HF6	[16,18]	•	301	•	368.7	•		–	370.2	•	371.7	•
6HF6	[16,18]	•	315	•	347	•		–	376.9	•	377.6	•
5FF6	[16,19]	•	327	•	380.3	•	380.7	•	381.5	•	382.3	•
6FF6	[16]	•	336	•	358	•		–	383.7	•	386.0	•

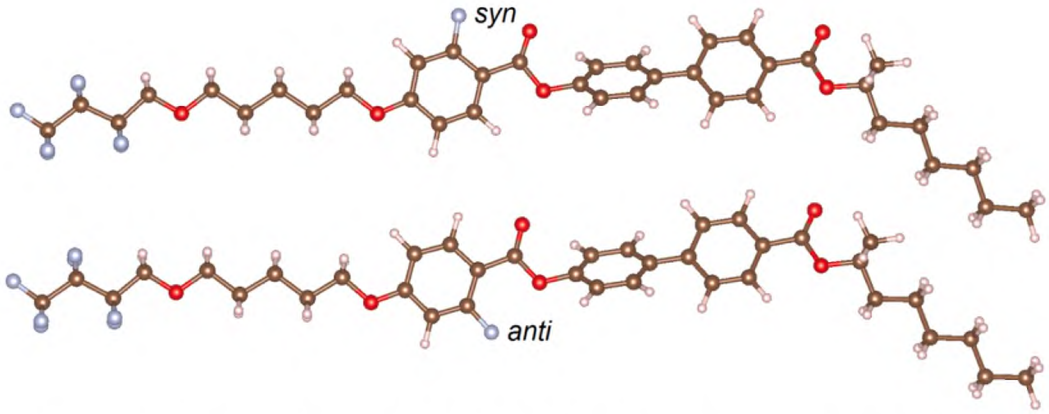

Fig. 2. 5HF6 molecule in the *syn* and *anti* conformations, optimized with the DFT + D3/BLYP-def2TZVP method.

crystallization of the 3FmX$_1$PhX$_2$6 compounds is still conducted because (1) the 3FmX$_1$PhX$_2$6 compounds serve as components of antiferroelectric mixtures which could be applicable in displays [16,22,23], (2) the vitrified chiral tilted smectic phases may potentially be used as optical filters, similarly as it had been presented for chiral nematics [24] and (3) the compounds which form the glass during cooling and exhibit cold crystallization after reheating are considered suitable for the purpose of energy storage [25].

2. Materials and methods

The investigated mX$_1$X$_2$6 compounds, the synthesis and purity analysis of which is described in Refs. [16,17], are:

- (*S*)-4′-(1-methylheptyloxycarbonyl) biphenyl-4-yl 4-[5-(2,2,3,3,4,4,4-heptafluorobutoxy) pentyl-1-oxy]-2-fluorobenzoate (5HF6),
- (*S*)-4′-(1-methylheptyloxycarbonyl) biphenyl-4-yl 4-[5-(2,2,3,3,4,4,4-heptafluorobutoxy) pentyl-1-oxy]-2,3-difluorobenzoate (5FF6),
- (*S*)-4′-(1-methylheptyloxycarbonyl) biphenyl-4-yl 4-[6-(2,2,3,3,4,4,4-heptafluorobutoxy) hexyl-1-oxy]-2-fluorobenzoate (6HF6),
- (*S*)-4′-(1-methylheptyloxycarbonyl) biphenyl-4-yl 4-[6-(2,2,3,3,4,4,4-heptafluorobutoxy) hexyl-1-oxy]-2,3-difluorobenzoate (6FF6).

IR spectra were collected in the 400–4000 cm^{-1} range with the resolution of 1 cm^{-1} (32 scans for each spectrum) using the Fourier-transform IR spectroscopy method (FT-IR) for the mX$_1$X$_2$6/KBr tablets on heating and subsequent cooling with Bruker VERTEX 70v vacuum spectrometer with Advanced Research System DE-202A cryostat and ARS-2HW water-cooled helium compressor.

Density functional theory (DFT) simulations of IR spectra were carried out with Gaussian09 [26] for isolated mX$_1$X$_2$6 molecules in two conformations differing in the position of the fluorine atom(s) with respect to the C═O group between the benzene ring and biphenyl; the two geometries have either the *syn* or *anti* conformations, wherein the F atom(s) and C═O group are either on the same side (*syn*) or on the opposite sides (*anti*) of the benzene ring (Fig. 2). The calculations were performed using the BLYP exchange–correlation functional [27,28] with the third-generation Grimme's set of semi-empirical dispersion corrections with the Becke-Johnson damping, D3 [29,30]. Two basis sets were examined: def2SVP and def2TZVP [31]. Identification of intramolecular vibrations was performed in Avogadro [32], while visualizations were done in Vesta [33].

3. Results and discussion

3.1. Bands assignment

A comparison between the experimental and calculated IR spectra for the mHF6 and mFF6 (m = 5, 6) compounds is shown in Fig. 3, wherein the experimental data is recorded in the crystal phase at room temperature and the calculated data is extracted from the DFT + D3/BLYP-def2SVP and DFT + D3/BLYP-def2TZVP molecular models. The

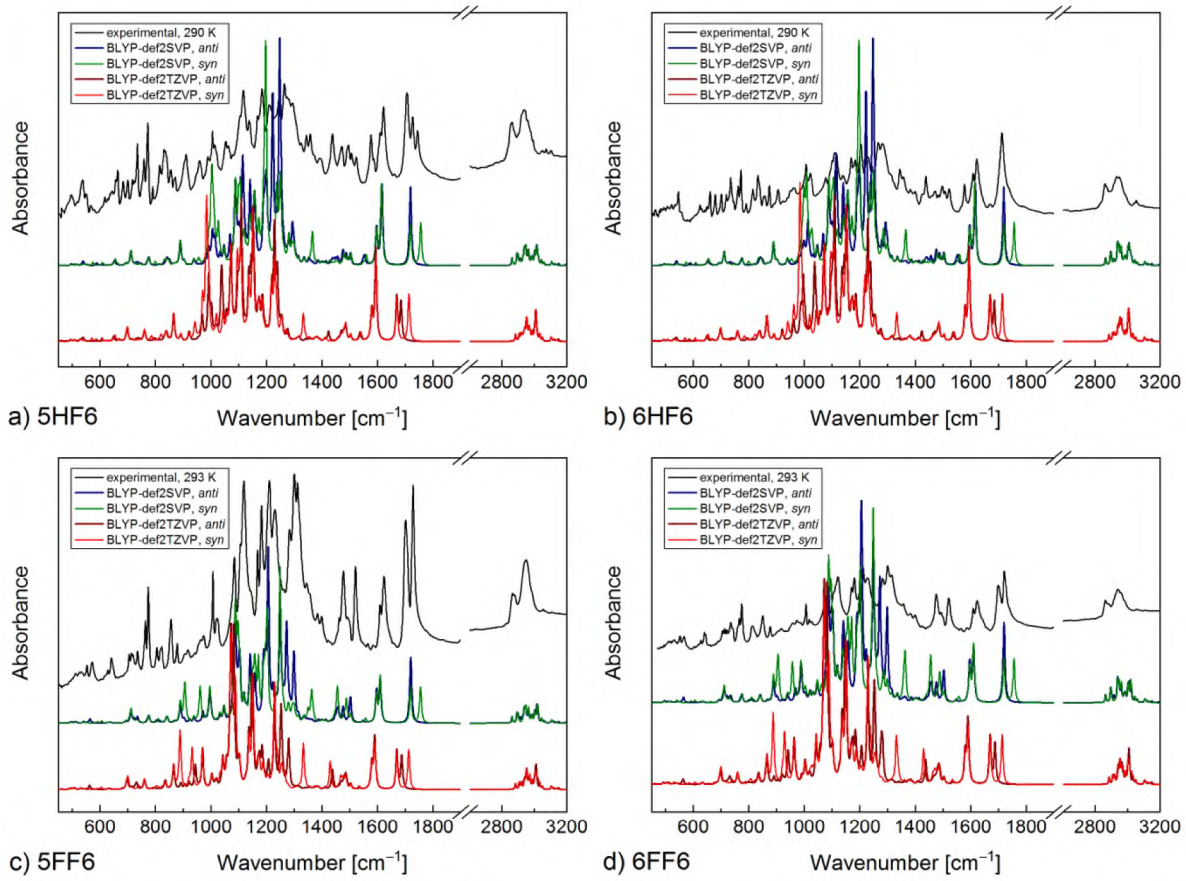

Fig. 3. Experimental IR spectra for four mX_1X_26 compounds (m = 5, 6; X_1 = H, F; X_2 = F) collected in the crystal phase at room temperature, compared with the IR spectra calculated with DFT + D3/BLYP-def2SVP and DFT + D3/BLYP-def2TZVP for two conformations (*anti* and *syn*, see Fig. 2).

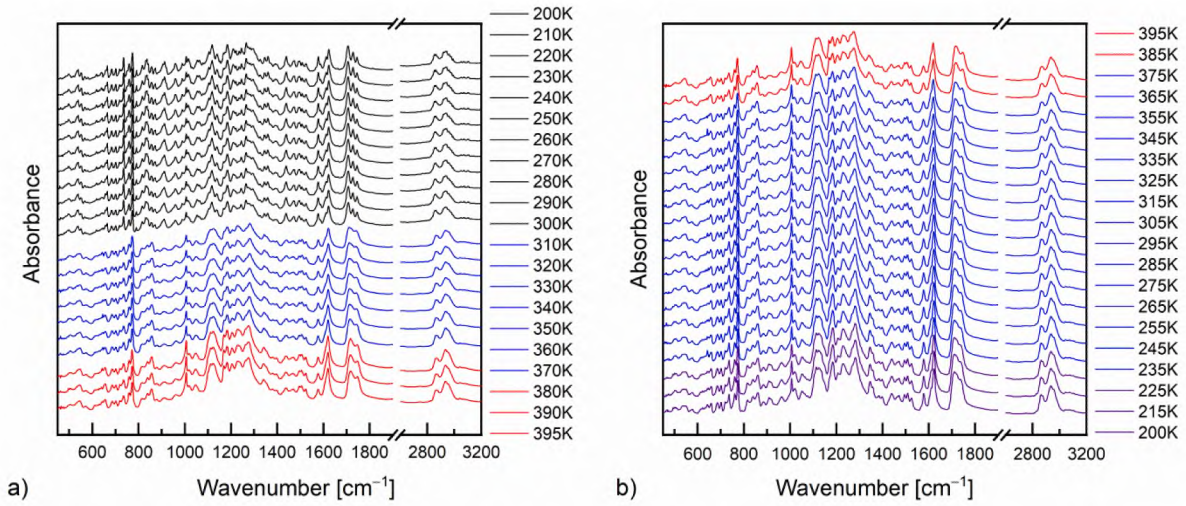

Fig. 4. FT-IR spectra of 5HF6 collected on heating (a) and subsequent cooling (b) in the temperature range 200–395 K.

temperature dependence of the experimental IR spectra for 5HF6 (on heating and cooling) is presented in Fig. 4, while corresponding results for other compounds are shown in the Supplementary Materials (SM) in Figures S1-S3. A meticulous analysis of the computed data, as presented in Table 2 and Fig. 5 for 5HF6, and Tables S1-S3 and Figures S4-S6 for the remaining examined compounds, shows that both of the applied basis sets provide very similar characterizations of the absorption bands, and that the band assignments do not differ significantly among the four considered mX_1X_26 compounds. All the calculated wavenumbers and intensities of IR absorption bands are attached as supplementary.txt files.

The bands in the 500–1000 cm^{-1} region can be assigned to the in-plane (β) and out-of-plane (γ) deformations of the aromatic rings. The vibrations involving atoms from the molecules' terminal chains are C—C, C—O and C-F stretching (ν), C—C—O, C—O—C, C—C—C, and CF_2 scissoring (δ), CH_2 and CF_2 wagging (ω), and CH_2 rocking (ρ). The

Table 2
Band assignments of the FT-IR spectrum for the 5HF6 compound in a crystal phase at 290 K, based on DFT + D3/BLYP-def2SVP and DFT + D3/BLYP-def2TZVP calculations performed for the isolated 5HF6 molecule in its *anti* and *syn* conformations (denoted with superscripts [a] and [s], respectively). The experimental and calculated wavenumbers are given in cm^{-1}. The symbols used are: β – in-plane deformation of the phenyl ring (Ph), γ – out-of-plane deformation of Ph, ν – stretching, δ – scissoring, ρ – rocking, τ – twisting, ω – wagging. The letters (a)-(j) denote the particular fragments of the molecule as shown in Fig. 1. Compare with Fig. 3. See SM for the corresponding data for the remaining compounds.

Experimental	BLYP-def2SVP		BLYP-def2TZVP	
	Calculated	Assignment	Calculated	Assignment
497	496.3[a], 492.8 [s]	δCCC(j), δCCC(c)[s]	494.3[a], 496.1 [s]	δCCC(j), δCCC(c)
536	537.9[a]	β_{asym}Ph(d)	529.3[a], 530.5 [s]	δCF_2(a), δCOC(b,c), β_{asym}Ph(d)
	541.3[a], 541.0 [s]	δCF_2(a), δCOC(b,c), β_{asym}Ph(d)[a]	539.0[a]	β_{asym}Ph(d)
550	554.8[a], 552.3 [s]	γPh(f)Ph(g)	544.6[a], 544.7 [s]	γPh(f)Ph(g)
567	574.7 [s]	β_{asym}Ph(d)	570.9 [s]	β_{asym}Ph(d)
578	588.8[a]	β_{asym}Ph(d), β_{asym}Ph(f)	586.1[a]	β_{asym}Ph(d)
618	610.6[a], 609.0 [s]	β_{asym}Ph(d), β_{asym}Ph(f)Ph(g)	609.5[a], 606.7 [s]	β_{asym}Ph(d), β_{asym}Ph(f)Ph(g)
663	652.1[a], 654.9 [s]	β_{asym}Ph(d), anti-phase β_{asym}Ph(f)Ph(g)	649.5[a], 653.0 [s]	β_{asym}Ph(d), anti-phase β_{asym}Ph(f)Ph(g)
683	662.8[a], 664.7 [s]	γPh(d)	668.6[a], 668.5 [s]	γPh(d)
700				
717	693.3[a], 693.2 [s]	γPh(f)Ph(g)	693.8[a], 693.8 [s]	γPh(f)Ph(g)
735	711.4[a], 711.3 [s]	ωCF_2(a), δCCO(a,b)	698.8[a], 698.8 [s]	ωCF_2(a), δCCO(a,b)
758	735.4[a]	γPh(d), ρCH_2(c)	736.2[a]	γPh(d), ρCH_2(c)
772	776.2[a], 776.1 [s]	ωCF_2(a), νCC(a), δCCO(a,b)	758.9[a], 758.8 [s]	ωCF_2(a), νCC(a), δCCO(a,b)
790	799.9 [s]	γPh(f)Ph(g), ν_{sym}COC(e,f)	785.1 [s]	γPh(f)Ph(g), ν_{sym}COC(e,f)
816	832.4 [s]	γPh(d), ρCH_2(c)	820.2 [s]	γPh(d), ρCH_2(c)
831	841.8[a], 841.5 [s]	γPh(f)Ph(g), ρC*HCH_3(i), ρCH_2(j)	833.0[a], 833.2 [s]	γPh(f)Ph(g), ρC*HCH_3(i), ρCH_2(j)
855	845.9 [s]	γPh(f)Ph(g)	837.2[a]	γPh(d)
871	849.9[a]	γPh(d), ρCH_2(c)	841.2[a], 838.6 [s]	γPh(f)Ph(g)
910	889.5[a], 889.4 [s]	ωCF_2(a), ν_{sym}CCO(a,b), ωCH_2(b)	865.4[a], 865.5 [s]	ωCF_2(a), ν_{sym}CCO(a,b), ωCH_2(b)
959	955.9 [s]	β_{asym}Ph(d), ν_{sym}COC(c,d), νCC(c)	942.3 [s]	β_{asym}Ph(d), ν_{sym}COC(c,d), νCC(c), ν_{sym}CO(e)
989	991.6[a], 991.6 [s]	in-phase β_{asym}Ph(f)Ph(g), ν_{sym}COC(b,c), νCC(c), β_{asym}Ph(d)	968.2[a], 969.8 [s]	ν_{sym}COC(b,c), νCC(c), β_{asym}Ph(d)
1006	1000.5 [s]	anti-phase β_{asym}Ph(f)Ph(g)	983.9 [s]	β_{asym}Ph(d), ωCH_2(c), νCO(c), νCO(e)
	1003.2 [s]	τCH_2(j)		
	1006.4[a], 1004.7 [s]	ωCH_2(c), β_{asym}Ph(d)[a]	991.8[a], 990.9 [s]	β_{asym}Ph(d), ωCH_2(c), νCO(c), νCO(e)
1014	1014.4[a], 1010.2 [s]	νCC(c), β_{asym}Ph(d) in-phase β_{asym}Ph(f)Ph(g), ν_{sym}COC(b,c)[a], νCO(e)[s]	1001.6[a]	νCC(c), β_{asym}Ph(d) in-phase β_{asym}Ph(f)Ph(g)
1054	1025.9 [s]	νCC(c), νCO(e), in-phase β_{asym}Ph(f)Ph(g)	1019.6 [s]	in-phase β_{asym}Ph(f)Ph(g), νCC(j)
	1032.9[a]	νCC(j)	1036.7[a]	νCC(c), νCO(e)
			1039.4[a]	νCC(c), νCO(e)
1062	1047.0[a], 1047.0 [s]	ωC*HCH_3(i), ωCH_2(j)	1043.3[a], 1043.3 [s]	ωC*HCH_3(i), ωCH_2(j)
1105	1087.8[a], 1087.6 [s]	β_{asym}Ph(g), ν_{asym}COC*(h,i)	1072.4[a], 1072.3 [s]	β_{asym}Ph(g), ν_{asym}COC*(h,i)
1117	1114.5[a], 1106.2 [s]	β_{asym}Ph(d), ν_{asym}CCO(d,e)[a]	1110.0[a], 1107.9 [s]	β_{asym}Ph(d), ν_{asym}CCO(d,e)
1138	1119.5[a], 1119.4 [s]	$\nu_{asym}$$CF_2$(a), τ$CH_2$(b,c)		
1168	1140.4[a], 1140.4 [s]	$\nu_{sym}$$CF_2$(a), ν_{asym}COC(b,c), ρCH_2(c), β_{sym}Ph(f)[a]	1136.6[a], 1136.6 [s]	$\nu_{asym}$$CF_2$, τ$CH_2$(b,c), ρ$CH_2$(c)
	1141.6[a], 1150.1 [s]	β_{sym}Ph(f)	1144.6[a]	β_{asym}Ph(d), ν_{asym}CCO(d,e), β_{asym}Ph(f)
1184	1157.2[a], 1157.1 [s]	ρC*HCH_3(i), ρCH_2(j), β_{sym}Ph(g), β_{asym}Ph(d)[a]	1154.1[a], 1150.7 [s]	β_{asym}Ph(f), β_{asym}Ph(d)
			1152.5[a]	$\nu_{sym}$$CF_2$(a), νCC(a)
1211	1200.5[a], 1197.4 [s]	β_{asym}Ph(d), β_{asym}Ph(f), ν_{asym}CCO(d,e)[s]	1185.6[a], 1184.1[a]	in-phase β_{sym}Ph(f)Ph(g), ν_{asym}COC(e,f), β_{asym}Ph(d)
1244	1222.5[a], 1236.9 [s]	β_{asym}Ph(d), ν_{asym}CCO(d,e), β_{asym}Ph(f)	1217.7[a], 1218.4 [s]	β_{sym}Ph(d), ν_{asym}CCO(d,e), β_{asym}Ph(f)[s]
1265	1247.7[a]	β_{asym}Ph(d), ν_{asym}CCO(d,e), in-phase β_{asym}Ph(f)Ph(g), ν_{asym}CCO(g,h), τC*HCH_3(i), τCH_2(j)	1228.9[a]	β_{asym}Ph(g), ν_{asym}CCO(g,i), τC*HCH_3(i), ωCH_2(j)
1274	1250.0 [s]	β_{asym}Ph(g), ν_{asym}CCO(g,h), τC*HCH_3(i), τCH_2(j)	1229.7 [s]	β_{asym}Ph(g), ν_{asym}CCO(g,h), τC*HCH_3(i), ωCH_2(j)
1281	1253.2[a], 1253.1 [s]	τCH_2(b)	1235.6 [s]	β_{asym}Ph(d), ωCH_2(c)
1293	1253.5[a]	β_{asym}Ph(d), ν_{asym}CCO(d,e), anti-phase β_{asym}Ph(f)Ph(g), ν_{asym}CCO(g,h), τC*HCH_3(i), τCH_2(j)	1239.0[a]	β_{asym}Ph(d), ν_{asym}CCO(d,e), ωCH_2(c)
1325	1262.2[a], 1262.4 [s]	ωC*HCH_3(i), ωCH_2(j)	1251.9[a], 1251.9 [s]	τCH_2(b)
1344	1280.0[a], 1280.8 [s]	in-phase β_{asym}Ph(f)Ph(g), ωCH_2(c)[s], β_{asym}Ph(d)[s]	1256.3[a], 1256.3 [s]	$\nu_{sym}$$CF_2$(a), νCC(a), ω$CH_2$(c)
1358	1293.8[a], 1291.9 [s]	ωCH_2(c), β_{asym}Ph(d)[a], τCH_2(j)[s]	1276.7[a], 1270.9 [s]	β_{asym}Ph(d), ωCH_2(c), anti-phase β_{asym}Ph(f)Ph(g)[a]
	1299.1[a], 1298.9 [s]	$\nu_{sym}$$CF_2$(a), νCC(a), ω$CH_2$(b)		
1393	1365.3 [s]	β_{asym}Ph(d)	1332.9 [s]	β_{asym}Ph(d)

(*continued on next page*)

Table 2 (*continued*)

Experimental	BLYP-def2SVP		BLYP-def2TZVP	
	Calculated	Assignment	Calculated	Assignment
1438	1437.8[a], 1428.2 [s]	β_{asym}Ph(d), δCH_2(c), ωCH_2(c)[s]	1424.0[a], 1413.1 [s]	β_{asym}Ph(d), ωCH_2(c)
1471	1457.0[a], 1456.0 [s]	δCH_2(b,c)	1458.4[a], 1458.5 [s]	δCH_2(b,c)
1495	1475.7[a], 1478.9 [s]	in-phase β_{asym}Ph(f)Ph(g)	1470.1[a], 1470.2 [s]	δCH_2(b,c), β_{asym}Ph(d)
1507	1487.7[a], 1491.0 [s]	β_{asym}Ph(d), δCH_2(c)	1484.5[a], 1484.8 [s]	in-phase β_{asym}Ph(f)Ph(g), δCH_2(b,c)
1524	1502.6[a], 1504.5 [s]	anti-phase β_{asym}Ph(f)Ph(g)	1503.5[a], 1503.6 [s]	anti-phase β_{asym}Ph(f)Ph(g)
1577	1547.4[a], 1548.9 [s]	anti-phase β_{asym}Ph(f)Ph(g)	1535.9[a], 1535.8 [s]	anti-phase β_{asym}Ph(f)Ph(g)
1586	1552.9[a], 1559.4 [s]	β_{asym}Ph(d)	1537.4[a], 1540.3 [s]	β_{asym}Ph(d)
1611	1596.5[a], 1596.3 [s]	in-phase β_{sym}Ph(f)Ph(g)	1579.5[a], 1579.6 [s]	in-phase β_{sym}Ph(f)Ph(g)
1622	1615.7[a], 1614.2 [s]	β_{sym}Ph(d)	1594.0[a], 1594.4 [s]	β_{sym}Ph(d)
1706	1718.0[a], 1718.9 [s]	anti-phase $\nu C=O$(e) and $\nu C=O$(h)[a], $\nu C=O$(h)[s]	1669.7[a], 1669.9 [s]	$\nu C=O$(h)
1727	1719.3[a]	in-phase $\nu C=O$(e) and $\nu C=O$(h)[a]	1684.9[a]	$\nu C=O$(e)
1746	1755.8 [s]	$\nu C=O$(e)[s]	1713.4 [s]	$\nu C=O$(e)
2862	2938.1[a], 2938.0 [s]	ν_{sym}CH(j)	2954.3[a], 2954.3 [s]	ν_{sym}CH(j)
	2945.9[a], 2945.9 [s]	ν_{sym}CH(j)		
	2948.2[a], 2948.1 [s]	ν_{sym}CH(j), ν_{asym}CH(j)		
2938	3001.9[a], 3001.8 [s]	ν_{asym}CH(j)	3001.4[a], 3001.5 [s]	νCH(i), ν_{asym}CH(j)
	3013.2[a], 3013.2 [s]	ν_{asym}CH(c)	3008.3[a], 3008.4 [s]	ν_{asym}CH(j)
	3016.7[a], 3016.8 [s]	ν_{asym}CH(j)	3009.2[a], 3009.1 [s]	ν_{asym}CH(c)

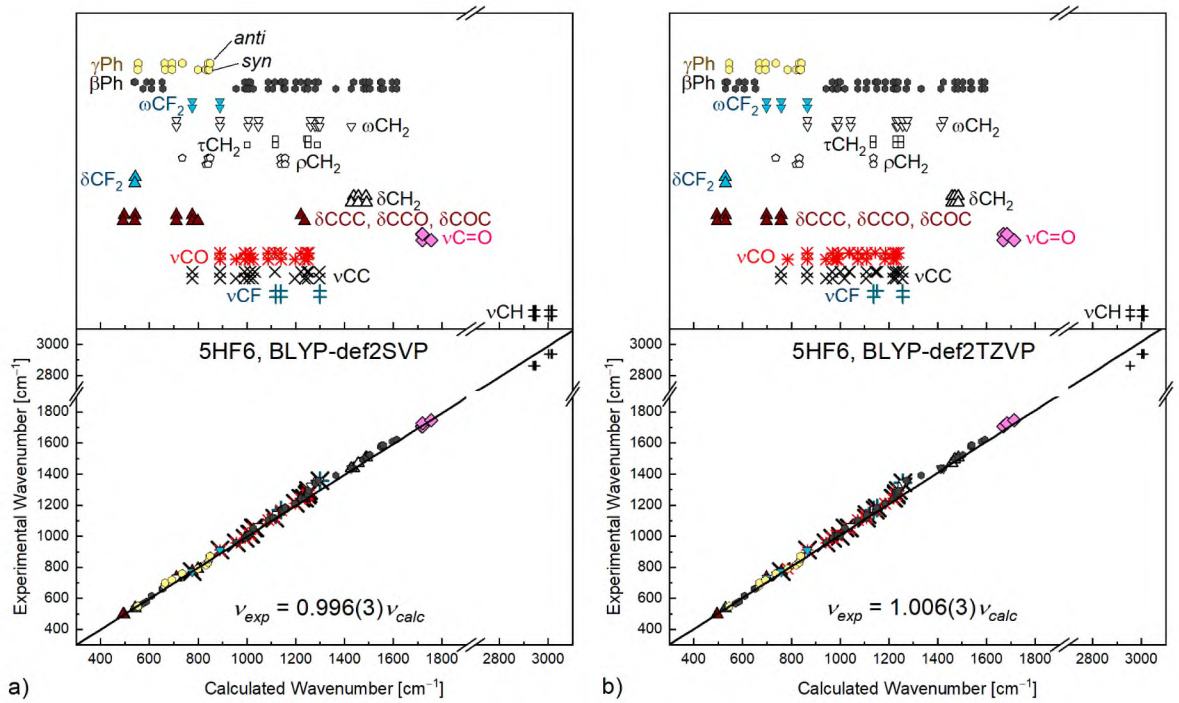

Fig. 5. Band assignments and the experimental vs. calculated wavenumbers obtained using DFT + D3 calculations with BLYP-def2SVP and BLYP-def2TZVP for 5HF6 in both *anti* and *syn* conformation. See Table 2 for the numerical data and SM for the corresponding data for the remaining compounds.

1000–1550 cm^{-1} range contains bands related to the β deformations of benzene rings as well as the stretching of C—C, C—O and C—F bonds and various vibrations (δ, ω, ρ, and τ – twisting) involving the CH_2 groups. The bands in the 1550–1650 cm^{-1} region are related to the in-plane symmetric deformations (β_{sym}) of the C—C bonds in the aromatic rings. The β_{sym} vibrations of the fluorinated benzene ring (Ph(d))

Table 3
Scaling coefficient a between experimental ν_{exp} and calculated ν_{calc} wavenumbers, determined from the linear fit $\nu_{exp} = a\nu_{calc}$ (Fig. 4 and Figures S5-S7 in SM).

compound	BLYP-def2SVP	BLYP-def2TZVP
5HF6	0.996(3)	1.006(3)
6HF6	0.994(3)	1.003(3)
5FF6	0.996(3)	1.013(3)
6FF6	0.994(3)	1.011(4)

contribute mostly to the bands at higher wavenumbers of this range, while the β_{sym} vibrations of the biphenyl (Ph(f)Ph(g)) contribute rather to the bands at lower wavenumbers. The β_{sym}Ph(d) vibrations are coupled with the weak ωCH_2(c) and νC═O(e) vibrations. The contribution of the νC═O(h) vibration, coupled with β_{sym}Ph(g), is negligible. The bands located in the 1650–1800 cm^{-1} range are related to the νC═O vibrations (see Section 3.2). Finally, the 2800–3000 cm^{-1} region contains bands related to the νCH vibrations in the chiral chain. The bands arising from asymmetric C—H stretching are observed at higher wavenumbers than these related to symmetric C—H stretching.

The values of a scaling coefficient a between the experimental ν_{exp} and calculated ν_{calc} wavenumbers [34] for both applied basis sets are presented in Table 3. For the def2SVP basis set, $a = 0.994–0.996$ with an uncertainty equal to 0.003 for all compounds, therefore the ν_{calc} values are in general slightly overestimated compared to ν_{exp}. The visible exception are the ν_{calc} wavenumbers related to the νCH vibrations, which are underestimated. For the def2TZVP basis set, the scaling coefficient exceeds 1 and equals 1.003–1.006 for mHF6 and 1.011–1.013 for mFF6, with an uncertainty of 0.003–0.004. It means that the ν_{calc} values are underestimated compared to ν_{exp}, especially for mFF6 compounds. However, in both cases the scaling coefficient is close to 1, which indicates a good agreement of the ν_{exp} and ν_{calc} wavenumbers.

3.2. Stretching of the C═O bonds vs. Temperature

The bands in the 1650–1800 cm^{-1} region, which originate from the νC═O stretching, show a visible dependence of their wavenumbers on temperature (Fig. 6), therefore they have been selected for detailed analysis. The fitting with several Gaussian or pseudo-Voigt peak functions reveals four components in this spectral region for the samples in the isotropic liquid or smectic phases, however, the wide maximum on the high-wavenumber side is treated as a background contribution. The three main components are denoted as I, II, III in the order of the increasing wavenumber. The DFT + D3 calculations at the BLYP-def2SVP and BLYP-def2TZVP levels of theory give slightly different interpretations of these bands, although they both indicate a significant impact of the position of the F atom(s) substituted to the benzene ring on the νC═O vibration in the COO group within the molecular core. To recall, the theoretical spectra were simulated for two conformations of each mX_1X_26 molecule: the *anti* conformation, in which the F atom(s) and the neighboring C═O group are on the opposite sides of the benzene ring, and the *syn* conformation, in which the F atom(s) and the aforementioned C═O group are adjacent to each other (Fig. 2).

The BLYP-def2SVP results for the *anti* conformation give in this spectral region two bands centered at almost the same wavenumber, which, when visualized, appear as anti-phase νC═O (lower wavenumber) and in-phase νC═O (higher wavenumber) modes of the two C═O groups, i.e. the two νC═O vibrations have similar frequencies and appear coupled. For the *syn* conformation, on the other hand, these

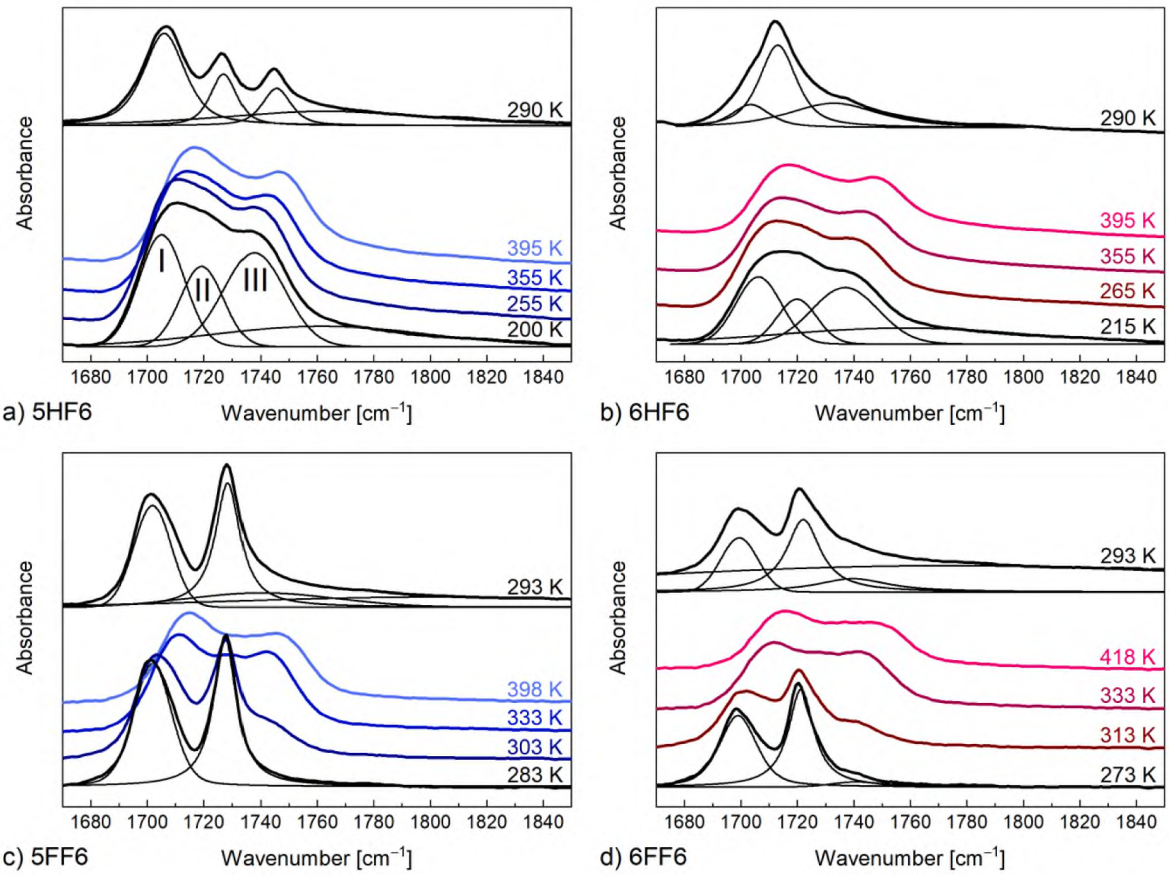

Fig. 6. FT-IR spectra in the wavenumber region of the C═O stretching bands collected in room temperature before the first melting (top) and on cooling from the isotropic liquid (bottom) for 5HF6 (a), 6HF6 (b), 5FF6 (c) and 6FF6 (d). The fitting results are presented for the top and bottom spectra in each panel. For 5HF6, the notation I, II, III or the bands is presented (the fourth, wide peak is treated as a background).

Table 4
Energy difference [kJ/mol] between the *syn* and *anti* conformations of the $mX_1X_2$6 molecules.

compound	BLYP-def2SVP	BLYP-def2TZVP
5HF6	2.1	1.4
6HF6	2.2	1.6
5FF6	6.1	9.3
6FF6	6.6	10.0

bands become 'decoupled' when visualized, with the lower-wavenumber band and the higher-wavenumber band corresponding to νC═O in the COO group close to the chiral center and close to the fluorinated benzene ring, respectively.

In the spectra calculated with BLYP-def2TZVP, the νC═O vibrations are decoupled for both *anti* and *syn* conformations, with the same origin of the bands as described above, i.e. the band related to νC═O in the COO group close to the chiral center is characterized by a lower wavenumber than the band stemming from νC═O in the COO group close to the fluorinated benzene ring. While the former band, as expected, seems not to be affected by the relative position of the F atom(s) and the COO group attached to the same benzene ring, and it is observed at the same wavenumber for both *syn* and *anti* conformations, the latter band is shifted to the higher wavenumbers for the *syn* conformation as compared to *anti*. Qualitatively the same results to the one presented here for the DFT + D3/BLYP-def2TZVP method were previously obtained with DFT/BLYP-DGauss [6], although the latter approach appears to overestimate the calculated wavenumbers with respect to the experimental wavenumbers.

Comparing the experimental and calculated IR spectra in the 1650–1800 cm^{-1} range, it can be thus assumed that the experimental band I is related to νC═O in the COO group close to the chiral center, while bands II and III correspond to νC═O in the COO group located in the molecular core associated with the molecules in *anti* and *syn* conformations, respectively. For all four considered compounds in the isotropic liquid and smectic phases, one can always observe the aforementioned I, II, III νC═O band components, which can be interpreted as a co-existence of both *syn* and *anti* molecular conformations. According to DFT results, the *anti* conformation is more energetically favorable, but the conformational energy of the *syn* conformation is not significantly higher; the difference is 1.4–10.0 kJ/mol, larger for mFF6 than for mHF6 (see Table 4). On the other hand, calculations for dimer and trimer models performed previously for the 7FF6 compound [15] show that splitting of the νC═O bands can be caused not only by intramolecular interactions, but also by interactions of the C═O group from one molecule with the F atom(s) from a neighboring molecule. Nevertheless, the dielectric spectroscopy results for the $mX_1X_2$6 compounds imply that rotations within the molecular core may occur in the vitrified SmC_A* phase or even in the crystal phase [10,21,35], therefore it is even more probable that conversions between the *syn* and *anti* conformations occur also above the melting temperature.

The wavenumbers of the νC═O bands identified in the 1650–1800 cm^{-1} region are presented in Fig. 7 as a function of temperature. The as-synthesized 5HF6 and 6HF6 samples (i.e. not melted after synthesis) cooled down to 200 K and 210 K, respectively, are in the crystal phase. In such a phase, for both homologues, three νC═O bands are observed, although for 5HF6 the bands are all narrow and of similar area, so they

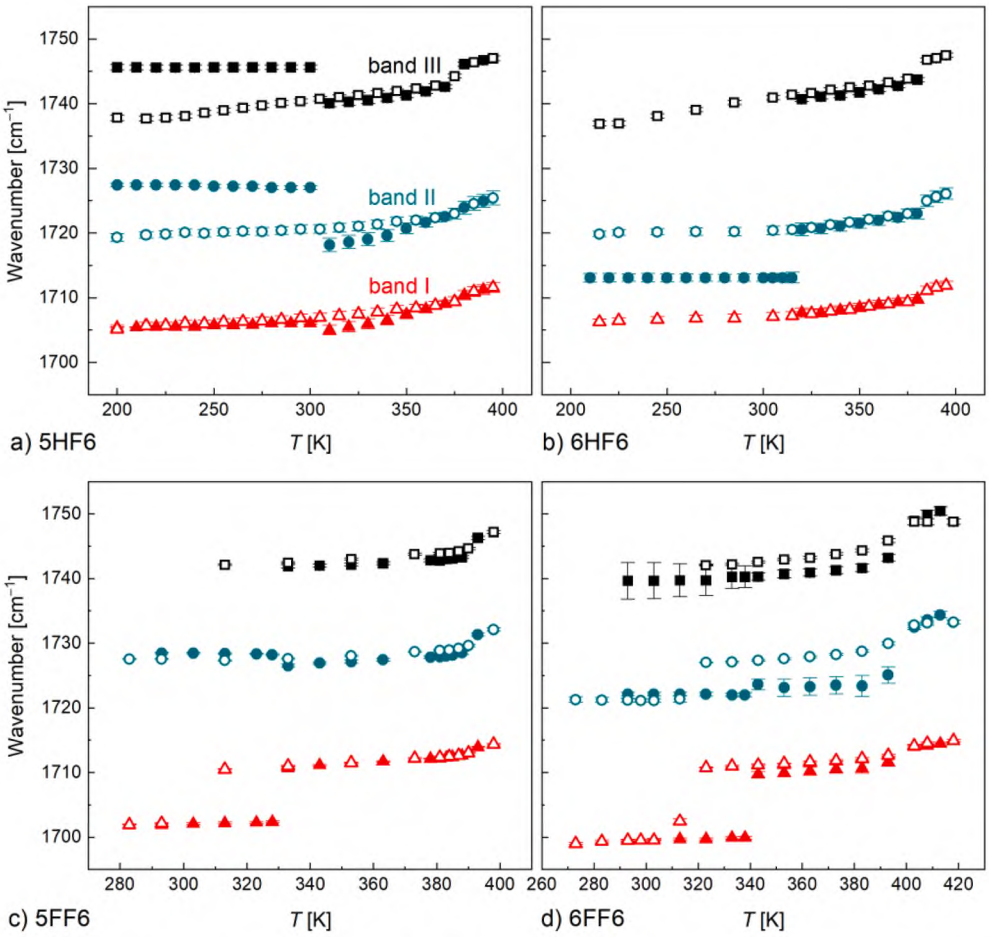

Fig. 7. Temperature dependence of the experimental wavenumbers of three absorption bands related to the C═O stretching in the mHF6 and mFF6 (m = 5, 6) molecules. The results from heating and cooling are presented by solid and open symbols, respectively.

can be easily deconvolved, while for 6HF6 only the strongest νC═O band II could be analyzed in detail, as the parameters for the weaker bands I and III were determined with significant uncertainties and accordingly they are not presented. In the crystal phases of 5FF6 and 6FF6, on the other hand, there are only two main absorption bands in the considered range, which indicates that rotations of the benzene rings are hindered. The third, weak band is caused rather by inter-molecular interactions than by the conformational disorder. Both 5FF6 and 6FF6 undergo the crystallization on cooling. The spectra observed for the freshly crystallized samples in the 1650–1800 cm^{-1} region are similar to the ones registered for the as-synthesized samples before the first melting. The small differences may arise from different crystal morphologies or number of defects, as the 5FF6 and 6FF6 crystals upon the samples syntheses were formed via growth from solution [17], while during the FT-IR measurements the crystals were formed via growth from the melt.

The melting of all investigated compounds on heating and crystallization of 5FF6 and 6FF6 on cooling are well visible in the IR spectra as the discontinuous changes in the wavenumber of at least one νC═O band. In the smectic phases and isotropic liquid phase, three νC═O bands are observed for all investigated compounds. The wavenumber of the band III is not affected by the fluorosubstitution at the X_1 position within the experimental uncertainties, while the bands I and II are blueshifted (shifted towards higher wavenumbers) for the mFF6 compounds compared to mHF6 (Table 5), as it was observed also for 7HF6 and 7FF6 [14]. This effect is very weak (no larger than a few cm^{-1}) and arises likely from inter-molecular interactions, as the DFT calculations in most of cases presume very close wavenumbers of the νC═O bands for the isolated mHF6 and mFF6 molecules in the same conformation (differences smaller than 1.5 cm^{-1}). Only the BLYP-def2TZVP results for the band II indicate the blueshift of 2.6 cm^{-1} for mFF6 compared to mHF6. In the smectic phases, the νC═O bands shift towards higher wavenumbers with increasing temperature, with a discontinuity at the clearing temperature (transition to the isotropic liquid). The transitions between the smectic phases are not visible in the temperature behavior of the νC═O bands. On subsequent cooling, the νC═O bands shift back towards lower wavenumbers. One can see that the parameters of the νC═O bands in the smectic phases are not identical on heating and cooling. It is attributed to the effect of the alignment within the samples, which can be different after melting of a crystal and after cooling from an isotropic liquid. The corresponding areas and half-widths of the absorption peaks, presented in Figures S7 and S8, are less informative because they are more significantly affected by the change in the samples' orientation, caused by heating to isotropic liquid and subsequent cooling. This is why only wavenumbers are used in the analysis.

The 5HF6 and 6HF6 homologues show the glass transition of the SmC_A* phase on cooling at $T_g \approx 230$ K, which, as it can be seen in Fig. 7, is noticeable very subtly in the temperature behavior of the band III with the highest wavenumber (C═O stretching in the COO group in the molecular core, *syn* conformation). Namely, this band shows the most significant redshift (shift towards lower wavenumbers) with decreasing temperature; it can however be noted that below T_g, its wavenumber remains rather constant. Constant position of the band III below T_g was observed also for the 7HF6 homologue, while in such a case, bands I and II were shown to demonstrate a redshift with decreasing temperature both before and after the glass transition, without any anomalies at T_g [15].

The C═O groups can be possibly involved in the formation of weak hydrogen bonds with the hydrogens from the aliphatic chains or benzene rings, as it was reported for other mesogenic compounds in their crystal phases [36–38]. The redshift of the νC═O bands can be interpreted as formation of new hydrogen bonds with decreasing temperature [1–3]. Interestingly, for the 7HH7 compound, without fluorosubstitution of the benzene ring and with a longer C_rH_{2r+1} chain, the glass transition of the SmC_A* phase leads to much more significant changes in the two observed νC═O bands, which show below T_g a step-like redshift of 6 cm^{-1} and 14 cm^{-1} for the band at lower and higher wavenumber, respectively [9]. It suggests that the glass transition of 7HH7 is related to the formation of the considerable amount of the hydrogen bonds involving both C═O groups. Such situation is not the case for mHF6 (m = 5, 6, 7), because no step-like redshift is observed at T_g (this work and [15]). For the 5HH7 compound, which is a homologue of 7HH7 with a shorter non-chiral chain and which shows the vitrification of the more ordered, hexatic SmX_A* phase, there is also a step-like change of the wavenumbers of νC═O bands at T_g. However, only the higher-wavenumber νC═O band shows a redshift of ca. 2 cm^{-1}, while the lower-wavenumber νC═O band show a blueshift of ca. 4 cm^{-1} below T_g [12], therefore the interpretation is not as straightforward as for 7HH7. These results suggest that the vitrification of the SmC_A* (or SmX_A*) phase may involve different inter-molecular interactions depending on the molecular structure. It shows the necessity of further systematic studies of the vibrational spectra for the mX_1X_2r glassformers.

4. Conclusions

The FT-IR spectroscopy was applied to investigate the intramolecular vibrations for four liquid crystalline compounds exhibiting the chiral smectic phases. It is shown that the length of the C_mH_{2m} non-chiral chain (m = 5, 6) does not have a significant influence on the observed IR spectra, which is confirmed by the DFT calculations, incorporating the BLYP functional and two basis sets, def2SVP or def2TZVP. The more important factor is the fluorosubstitution of the benzene ring, which, for the investigated compounds, is at 2-position (mHF6 homologues) or at the 2,3-positions (mFF6 homologues). Both the BLYP-def2SVP and BLYP-def2TZVP calculations confirm that the proximity of the F atom(s) from the benzene ring blueshifts one of the C═O stretching bands. Employment of the def2SVP basis set appears to better reproduce the experimental wavenumbers in an overall sense,

Table 5
Experimental (at temperature $T \approx 340$ K – SmC_A* phase) and calculated wavenumbers, given in cm^{-1}, of the νC = O bands for the mHF6 and mFF6 compounds. The superscripts [a] and [s] denote the *anti* and *syn* conformations, respectively.

compound	T [K]	experimental	BLYP-def2SVP	BLYP-def2TZVP
5HF6	340	1706.5(8)	1718.0[a], 1718.9 [s]	1669.7[a], 1669.9 [s]
		1719.6(1.0)	1719.3[a]	1684.9[a]
		1740.9(5)	1755.8 [s]	1713.4 [s]
6HF6	340	1708.1(7)	1718.1[a], 1718.9 [s]	1669.7[a], 1669.9 [s]
		1721.1(8)	1719.3[a]	1685.0[a]
		1741.2(4)	1755.9 [s]	1713.5 [s]
5FF6	343	1711.1(1)	1718.7[a], 1719.1 [s]	1670.0[a], 1670.1 [s]
		1726.9(2)	1720.7[a]	1687.5[a]
		1742.0(2)	1755.0 [s]	1712.6 [s]
6FF6	343	1709.7(5)	1718.7[a], 1719.1 [s]	1669.9[a], 1670.1 [s]
		1723.6(9)	1720.8[a]	1687.5[a]
		1740.3(6)	1755.4 [s]	1712.9 [s]

however, it also results in less blueshift of the affected C═O stretching mode (which, in the case of the *anti* conformation, results in the appearance of coupling between the νC═O vibrations). Meanwhile, the def2TZVP basis set yields wavenumbers that are generally lower than the experimental wavenumbers, but the differences in the two C═O stretching modes is more pronounced, and this is qualitatively closer to the experimental results. The detailed investigation of the νC═O bands vs. temperature shows that the most significant changes occur during the melting and crystallization processes. The smectic/isotropic liquid transition leads to much smaller changes in the νC = O bands than the crystal/smectic transition, and transitions between the smectic phases do not visibly affect the IR spectra. The redshift of the νC═O bands with decreasing temperature implies the increased role of hydrogen bonding between molecules. The cited results for the 7HH7 and 5HH7 compounds [9,12], where step-like changes in the positions of the νC═O bands are observed at the glass transition temperature of the SmC_A^* or hexatic SmX_A^* phases, suggest that formation of the hydrogen bonds may play some role in the glass transition. However, for two glass-forming mHF6 compounds investigated in this paper, the vitrification of the SmC_A^* phase is very weakly visible in the IR spectra, which shows that even for the compounds with very similar molecular structures, the glass transition may occur differently.

Declaration of Competing Interest

The authors declare that they have no known competing financial interests or personal relationships that could have appeared to influence the work reported in this paper.

Data availability

Data will be made available on request.

Acknowledgement

Bruker VERTEX 70v FT-IR spectrometer with Advanced Research System DE-202A cryostat and ARS-2HW compressor were purchased thanks to the European Regional Development Fund in the framework of the Innovative Economy Operational Program (contract no. POIG.02.01.00-12-023/08). The PL-Grid Infrastructure and the ACC Cyfronet AGH (Kraków, Poland) are acknowledged for providing computational resources.

Appendix A. Supplementary material

Supplementary data to this article can be found online at https://doi.org/10.1016/j.chemphys.2023.111977.

References

[1] P.J. Tonge, R. Fausto, P.R. Carey, FTIR studies of hydrogen bonding between α, β-unsaturated esters and alcohols, J. Mol. Struct. 379 (1996) 135–142, https://doi.org/10.1016/0022-2860(95)09117-3.

[2] E. Žagar, J. Grdadolnik, An infrared spectroscopic study of H-bond network in hyperbranched polyester polyol, J. Mol. Struct. 658 (2003) 143–152, https://doi.org/10.1016/S0022-2860(03)00286-2.

[3] Y. Liu, J. Zhao, Y. Peng, J. Luo, L. Cao, X. Liu, Comparative study on the properties of epoxy derived from aromatic and heteroaromatic compounds: the role of hydrogen bonding, Ind. Eng. Chem. Res. 59 (2020) 1914–1924, https://doi.org/10.1021/acs.iecr.9b05904.

[4] K. Drużbicki, A. Kocot, E. Mikuli, M.D. Ossowska-Chruściel, J. Chruściel, Temperature-dependent infrared spectroscopy studies of a novel antiferroelectric liquid-crystalline thiobenzoate, J. Phys. Chem. B 116 (2012) 11332–11343.

[5] E. Juszyńska-Gałązka, W. Zając, K. Saito, Y. Yamamura, N. Juruś, Vibrational dynamics of glass forming: 2-phenylbutan-1-ol (BEP), 2-(trifluoromethyl)phenethyl alcohol (2TFMP) and 4-(trifluoromethyl)phenethyl alcohol (4TFMP) in their thermodynamic phases, Phase Trans. 91 (2018) 170–185, https://doi.org/10.1080/01411594.2017.1393813.

[6] A. Drzewicz, A. Bombalska, M. Tykarska, Impact of molecular structure of smectogenic chiral esters ($3FmX_1X_2r$) on vibrational dynamics as seen by IR and Raman spectroscopy, Liq. Cryst. 46 (2019) 754–771, https://doi.org/10.1080/02678292.2018.1527959.

[7] N. Osiecka-Drewniak, M.A. Czarnecki, Z. Galewski, Investigation of phase transitions in liquid crystal 12BBAA using window clustering of infrared spectra, J. Mol. Liq. 341 (2021), 117233, https://doi.org/10.1016/j.molliq.2021.117233.

[8] A. Drzewicz, E. Juszyńska-Gałązka, W. Zając, M. Piwowarczyk, W. Drzewiński, Non-isothermal and isothermal cold crystallization of glass-forming chiral smectic liquid crystal (S)-4′-(1-methyloctyloxycarbonyl) biphenyl-4-yl 4-[7-(2,2,3,3,4,4,4-heptafluorobutoxy) heptyl-1-oxy]-benzoate, J. Mol. Liq. 319 (2020), 114153, https://doi.org/10.1016/j.molliq.2020.114153.

[9] A. Drzewicz, E. Juszyńska-Gałązka, W. Zając, P. Kula, Vibrational dynamics of a chiral smectic liquid crystal undergoing vitrification and cold crystallization, Crystals 10 (2020) 655, https://doi.org/10.3390/cryst10080655.

[10] A. Drzewicz, M. Jasiurkowska-Delaporte, E. Juszyńska-Gałązka, W. Zając, P. Kula, On the relaxation dynamics of a double glass-forming antiferroelectric liquid crystal, Phys. Chem. Chem. Phys. 23 (2021) 8673–8688, https://doi.org/10.1039/D0CP06203K.

[11] A. Dołęga, E. Juszyńska-Gałązka, N. Osiecka-Drewniak, P. Natkański, P. Kuśtrowski, A. Krupa, P.M. Zieliński, Study on the thermal performance of carbamazepine at different temperatures, pressures and atmosphere conditions, Thermochim. Acta 703 (2021), 178990, https://doi.org/10.1016/j.tca.2021.178990.

[12] A. Drzewicz, M. Jasiurkowska-Delaporte, E. Juszyńska-Gałązka, A. Deptuch, M. Gałązka, W. Zając, W. Drzewiński, On relaxation and vibrational dynamics in the thermodynamic states of a chiral smectogenic glass-former, Phys. Chem. Chem. Phys. 24 (2022) 4595–4612, https://doi.org/10.1039/D1CP05048F.

[13] A. Drzewicz, E. Juszyńska-Gałązka, M. Jasiurkowska-Delaporte, P. Kula, Insight into cold- and melt crystallization phenomena of a smectogenic liquid crystal, CrystEngComm 24 (2022) 3074–3087, https://doi.org/10.1039/D2CE00224H.

[14] T. Bezrodna, V. Nesprava, V. Melnyk, G. Klishevich, N. Curmei, T. Gavrilko, O. Roshchin, J. Baran, M. Drozd, Conformation-dependent molecular association and spectral properties of 4-pentyl-4'-cyanobiphenyl liquid crystal in different phases, Low Temp. Phys. 49 (2023) 329–337, https://doi.org/10.1063/10.0017240.

[15] A. Deptuch, A. Drzewicz, M. Dziurka, N. Górska, J. Hooper, T. Jaworska-Gołąb, E. Juszyńska-Gałązka, M. Marzec, M. Piwowarczyk, M. Srebro-Hooper, M. Tykarska, M. Urbańska, Influence of fluorosubstitution on physical properties of the smectogenic chiral ester, Mater. Res. Bull. 150 (2022), 111756, https://doi.org/10.1016/j.materresbull.2022.111756.

[16] M. Żurowska, R. Dąbrowski, J. Dziaduszek, K. Garbat, M. Filipowicz, M. Tykarska, W. Rejmer, K. Czupryński, A. Spadło, N. Bennis, J.M. Otón, Influence of alkoxy chain length and fluorosubstitution on mesogenic and spectral properties of high tilted antiferroelectric esters, J. Mater. Chem. 21 (2011) 2144–2153, https://doi.org/10.1039/C0JM02015J.

[17] M. Żurowska, R. Dąbrowski, J. Dziaduszek, K. Czupryński, K. Skrzypek, M. Filipowicz, Synthesis and mesomorphic properties of chiral esters comprising partially fluorinated alkoxyalkoxy terminal chains and a 1-methylheptyl chiral moiety, Mol. Cryst. Liq. Cryst. 495 (2008), https://doi.org/10.1080/15421400802432428, 145/[497]-157/[509].

[18] A. Deptuch, M. Marzec, T. Jaworska-Gołąb, M. Dziurka, J. Hooper, M. Srebro-Hooper, P. Fryń, J. Fitas, M. Urbańska, M. Tykarska, Influence of carbon chain length on physical properties of 3FmHPhF homologues, Liq. Cryst. 46 (2019) 2201–2212, https://doi.org/10.1080/02678292.2019.1614685.

[19] S. Lalik, A. Deptuch, P. Fryń, T. Jaworska-Gołąb, D. Dardas, D. Pociecha, M. Urbańska, M. Tykarska, M. Marzec, Systematic study of the chiral smectic phases of a fluorinated compound, Liq. Cryst. 46 (2019) 2256–2268, https://doi.org/10.1080/02678292.2019.1622044.

[20] P. Perkowski, W. Piecek, Z. Raszewski, K. Ogrodnik, J. Rutkowska, M. Żurowska, R. Dąbrowski, J. Kędzierski, X. Sun, New High Frequency Dielectric Mode in Fluorinated Antiferroelecteric Liquid Crystals, Ferroelectrics 365 (2008) 88–94, https://doi.org/10.1080/00150190802063666.

[21] A. Deptuch, E. Juszyńska-Gałązka, M. Jasiurkowska-Delaporte, A. Drzewicz, M. Piwowarczyk, M. Urbańska, Crystallization kinetics in the chiral compound showing the vitrification of the smectic C_A^* phase for moderate cooling rates, Phase Transitions 96 (2023) 166–185, https://doi.org/10.1080/01411594.2023.2168541.

[22] K. D'havé, P. Rudquist, S.T. Lagerwall, H. Pauwels, W. Drzewiński, R. Dąbrowski,, Solution of the dark state problem in antiferroelectric liquid crystal displays, Appl. Phys. Lett. 76 (2000) 3528–3530, https://doi.org/10.1063/1.126696.

[23] K. Agrahari, V.K. Nautiyal, T. Vimal, S. Pandey, S. Kumar, R. Manohar, Modification in different physical parameters of orthoconic antiferroelectric liquid crystal mixture via the dispersion of hexanethiol capped silver nanoparticles, J. Mol. Liq. 332 (2021), 115840, https://doi.org/10.1016/j.molliq.2021.115840.

[24] S.H. Chen, Multifunctional glassy liquid crystals for photonics, J. Soc. Inf. Disp. 12 (2004) 205–211, https://doi.org/10.1889/1.1825695.

[25] T. Ishikawa, A. Honda, K. Miyamura, Effects of alkyl chain length on the cold crystallization of Schiff-base nickel(II) complexes, CrystEngComm 24 (2022) 5900–5906, https://doi.org/10.1039/D2CE00305H.

[26] Gaussian 09, Revision A.02, M.J. Frisch, G.W. Trucks, H.B. Schlegel, G.E. Scuseria, M.A. Robb, J.R. Cheeseman, G. Scalmani, V. Barone, G.A. Petersson, H. Nakatsuji, X. Li, M. Caricato, A. Marenich, J. Bloino, B.G. Janesko, R. Gomperts, B. Mennucci, H.P. Hratchian, J.V. Ortiz, A.F. Izmaylov, J.L. Sonnenberg, D. Williams-Young, F. Ding, F. Lipparini, F. Egidi, J. Goings, B. Peng, A. Petrone, T. Henderson, D. Ranasinghe, V.G. Zakrzewski, J. Gao, N. Rega, G. Zheng, W. Liang, M. Hada, M. Ehara, K. Toyota, R. Fukuda, J. Hasegawa, M. Ishida, T. Nakajima, Y. Honda, O. Kitao, H. Nakai, T. Vreven, K. Throssell, J.A. Montgomery, J.E. Peralta, F. Ogliaro,

M. Bearpark, J.J. Heyd, E. Brothers, K.N. Kudin, V.N. Staroverov, T. Keith, R. Kobayashi, J. Normand, K. Raghavachari, A. Rendell, J.C. Burant, S.S. Iyengar, J. Tomasi, M. Cossi, J.M. Millam, M. Klene, C. Adamo, R. Cammi, J.W. Ochterski, R.L. Martin, K. Morokuma, O. Farkas, J.B. Foresman, D.J. Fox, Gaussian, Inc., Wallingford CT, 2016.

[27] A.D. Becke, Density-functional exchange-energy approximation with correct asymptotic behaviour, Phys. Rev. A 38 (1988) 3098–3100, https://doi.org/10.1103/PhysRevA.38.3098.

[28] C. Lee, W. Yang, R.G. Parr, Development of the Colle-Salvetti correlation-energy formula into a functional of the electron density, Phys. Rev. B 37 (1988) 785–789, https://doi.org/10.1103/PhysRevB.37.785.

[29] S. Grimme, J. Antony, S. Ehrlich, H. Kries, A consistent and accurate ab initio parametrization of density functional dispersion correction (DFT-D) for the 94 elements H-Pu, J. Chem. Phys. 132 (2010), 154104, https://doi.org/10.1063/1.3382344.

[30] S. Grimme, S. Ehrlich, L. Goerigk, Effect of the damping function in dispersion corrected density functional theory, J. Comput. Chem. 32 (2011) 1456–1465, https://doi.org/10.1002/jcc.21759.

[31] F. Weigend, R. Ahlrichs, Balanced basis sets of split valence, triple zeta valence and quadruple zeta valence quality for H to Rn: design and assessment of accuracy, Phys. Chem. Chem. Phys. 7 (2005) 3297–3305, https://doi.org/10.1039/B508541A.

[32] M.D. Hanwell, D.E. Curtis, D.C. Lonie, T. Vandermeersch, E. Zurek, G.R. Hutchison, Avogadro: an advanced semantic chemical editor, visualization, and analysis platform, J. Cheminf. 4 (2012) 17, https://doi.org/10.1186/1758-2946-4-17.

[33] K. Momma, F. Izumi, VESTA 3 for three-dimensional visualization of crystal, volumetric and morphology data, J. Appl. Cryst. 44 (2011) 1272–1276, https://doi.org/10.1107/S0021889811038970.

[34] A.P. Scott, L. Radom, Harmonic Vibrational Frequencies: An Evaluation of Hartree-Fock, Møller-Plesset, Quadratic Configuration Interaction, Density Functional Theory, and Semiempirical Scale Factors, J. Phys. Chem. 100 (1996) 16502–16513, https://doi.org/10.1021/jp960976r.

[35] A. Deptuch, M. Jasiurkowska-Delaporte, W. Zając, E. Juszyńska-Gałązka, A. Drzewicz, M. Urbańska, Investigation of crystallization kinetics and its relationship with molecular dynamics for chiral fluorinated glassforming smectogen 3F5HPhH6, Phys. Chem. Chem. Phys. 23 (2021) 19795–19810, https://doi.org/10.1039/D1CP02297K.

[36] J. Chruściel, B. Pniewska, M.D. Ossowska-Chruściel, The Crystal and Molecular Structure of 4-Pentylphenyl-4′-Pentioxythiobenzoate (5S5), Mol. Cryst. Liq. Cryst. 258 (1995) 325–331, https://doi.org/10.1080/10587259508034572.

[37] M.D. Ossowska-Chruściel, Z. Karczmarzyk, J. Chruściel, The Polymorphism Of 4-N-pentylphenyl-4'-N-butyloxythio-benzoate, (4OS5) in the crystalline state, Mol. Cryst. Liq. Cryst. 382 (2002) 37–52, https://doi.org/10.1080/713738755.

[38] A. Deptuch, T. Jaworska-Gołąb, J. Kusz, M. Książek, K. Nagao, T. Matsumoto, A. Yamano, M.D. Ossowska-Chruściel, Single crystal X-ray structure determination and temperature-dependent structural studies of the smectogenic compound 7OS5, Acta Cryst. B 76 (2020) 1128–1135, https://doi.org/10.1107/S2052520620014481.